Shear-triggered coalescence

Alireza Mashayekhi and Coralie Vazquez
Chemical and Biological Engineering, University of British Columbia, Canada V6T-1Z3

Hongying Zhao and Michael Gattrell
BC Research Inc., Richmond, British Columbia, Canada V6V-1M8

James F. Gilchrist
*Department of Chemical and Biomolecular Engineering, Lehigh University, Bethlehem,
Pennsylvania 18015, USA*

John M. Frostad
*Chemical and Biological Engineering, University of British Columbia, Canada V6T-1Z3
and Food Science, University of British Columbia, Canada V6T-1Z4*

Control over emulsion stability and phase separation is important for industries such as oil and gas, where it is critical to remove all the oil content from oily wastewater before discharging it into the environment or, conversely, to remove small droplets of water from oil prior to upgrading. Prior work has qualitatively shown that it may be possible for crude oil emulsions to be highly stable at rest and then rapidly destabilized by shearing interactions between droplets due to a phenomenon that we coin shear-triggered coalescence in this paper. In this paper, we provide quantitative evidence of this phenomenon using a cantilevered-capillary force apparatus to precisely manipulate two liquid droplets within another immiscible liquid (i.e., mineral oil in water or water in mineral oil). We first show that droplets in surfactant solutions clearly do not exhibit shear-triggered coalescence because they have the same probability of coalescing when a head-on collision of the droplets is compared to a shearing collision. In contrast, we show that when droplets have spherical Janus microparticles adsorbed onto the interface, the droplets undergoing shearing collisions coalesce faster than those undergoing a head-on collision. Similarly, we show that when rod-shaped nanoparticles (cellulose nanocrystals) are adsorbed onto the interface, with an intermediate salt concentration in the suspending phase, that shear-triggered coalescence occurs in dramatic fashion. We offer mechanistic explanations for why shear-triggered coalescence is possible in these two cases, but is not observed in other cases such as with disklike microparticles, non-Janus spherical microparticles, or rodlike nanoparticles without electrostatic screening or with strong electrostatic screening.

I. INTRODUCTION

An emulsion is a finely dispersed mixture of two or more immiscible liquids in which one liquid (dispersed phase) is dispersed as droplets within the other liquid (continuous or bulk phase). Due to their broad range of applications in various areas such as food, pharmaceutics, oil and gas, and agricultural industries, emulsions have drawn enormous attention. Most emulsions are thermodynamically unstable and eventually become phase separated via various mechanisms that

can be rapid or slow. This subject has attracted significant attention from researchers in several fields of research [1–6].

The known mechanisms of phase separation in emulsions include gravitational separation (sedimentation or creaming) and droplet-droplet interactions such as coalescence, Ostwald ripening, and aggregation [7]. In this paper, we focus our attention on coalescence. In a typical coalescence event, two liquid droplets approach each other, a thin film forms between the droplets (with or without significant deformation of the droplet shape), and the film drains until one of two things happens. First, the film may reach a critical film thickness where van der Waals forces dominate repulsive ones (e.g., electrostatic, steric, etc.) and the film ruptures, resulting in the two droplets merging into one [2]. Second, the film may reach a steady thickness where repulsive forces in the film (resulting in the so-called disjoining pressure) balance the collision force and coalescence happens more stochastically at some later time [8,9].

Researchers have employed various methods to study coalescence. One way of studying coalescence is to simply make an emulsion and monitor the droplet size distribution over time [10–16]. However, this method can offer only limited insight into the specific mechanisms that may influence coalescence, such as the rate and timescale of collisions between droplets, the occurrence of Ostwald ripening, etc. Furthermore, this method lacks the capability of visualizing microscale features, such as what happens in the thin film as droplets approach each other or whether the droplets coalesce during approach or separation in a glancing collision of droplets; knowledge of which is crucial for understanding coalescence. Thus, researchers have developed a wide variety of microscale methods in recent decades to gain more insight into coalescence [17–27], and some also attempt to directly compare the results of microscale and macroscale experiments [28,29].

The impetus for the present paper comes from an intriguing result obtained by Yeung *et al.* [24] when using a micropipette technique to study the coalescence of two bitumen droplets in simulated process water. In that study, when collided head-to-head, the droplets did not coalesce over a period of two minutes. The surprising result they found was that when the same two droplets collided in a shearing fashion (done by oscillating the droplets with an axial offset between the micropipettes), they coalesced very rapidly (after just two or three oscillations). The explanation for this result, which we term shear-triggered coalescence, was hypothesized to be related to nanoscale heterogeneity in the charge distribution on the surface of the droplets. In subsequent studies from the same group, evidence was provided in support of this hypothesis, but the results were not conclusive in establishing the mechanism [30,31].

Knowing that bitumen is a complex material containing high-molecular-weight compounds, saturates, naphthenic and polar aromatics, asphaltenes, and possibly trapped fine solid particles, one might suspect that other factors apart from surface charge heterogeneity could contribute to droplet coalescence under shear. For example, previous studies with bulk emulsions under shear have shown that solid, silica particles can act as emulsion breakers for both simple oil-in-water [32] as well as more complex bitumen-in-water [33] emulsions. In the former case, the effect was explained by the disruption of particle-droplet networks due to the flow field (higher shear rates corresponding to more destabilization), and in the latter it is related to droplet bridging by the particles to form a gel-like network of droplets. Somewhat similarly, proteins have been shown to act as emulsion stabilizers that then destabilize the emulsion during mixing due to rupture of the relatively rigid, and brittle, surface layers on the droplets [34,35].

Asphaltenes, in addition to being surface active at oil-water interfaces, are also known to form nanoaggregates and larger clusters depending on the concentration and oil composition [36–39]. Shi *et al.* showed that asphaltenes adsorbed at a toluene-water interface can result in adhesion between two droplets and that occasionally coalescence of two droplets appeared to be triggered by shearing of the droplets while in contact (similar to the study by Yeung *et al.*) [25,40]. They suggested that because the interfaces are viscoelastic that shearing could cause yielding in the interfacial structure and lead to coalescence. One strength of the work of Shi *et al.* is the relative simplicity of the

composition of the system compared to crude oil; however, the results related to shear-triggered coalescence were only qualitative.

Thus, in this paper, we hypothesize that shear-triggered coalescence can be reproduced in a system of lesser complexity for systematic study: e.g., a three- or four-component system. We further hypothesize that such a difference in coalescence time will not be observed for droplets stabilized by small-molecule surfactants, as this has not been verified in previous studies. By studying a simpler system, we expect that clarifying insight can be gained about the mechanism responsible for shear-triggered coalescence. If successful, this has the potential to provide a low-cost and practical tool to destabilize emulsions effectively in cases where emulsion breaking is crucial, such as in crude oil processing.

II. MATERIALS AND METHODS

A. Materials

Puretol 6 Mineral Oil (Petro-Canada Lubricants Inc., Canada) and ultrapure water with 18.2 M$\Omega \cdot$ cm resistivity, obtained from an Elga purification system, were used as the oil and water phases. Sodium dodecyl sulfate (Fisher Scientific, electrophoresis grade), Span 80 (TCI America), and Triton X-165 (Sigma-Aldrich) were used as surfactants to stabilize emulsion droplets. Sodium chloride, sodium sulfate, and sodium bicarbonate (Fisher Scientific) were used to screen electrostatic charges and make simulated process water.

Sulfonated cellulose nanocrystals (CNCs) were purchased from Celluforce (Canada, Montreal, QC). 300 mL dispersions of 0.5 wt % CNC were first stirred for at least three hours in a 500 mL beaker with a 45×8 mm magnetic stirrer at 150 RPM until all visible CNC aggregates disappeared. The CNC dispersion was then probe-sonicated for a total time of 15 minutes with 60% amplitude on an SFX550 Branson sonifier with a 1/8" microtip (Branson Ultrasonic Canada, Markham, ON). Sonication was done in an ice bath to prevent CNC desulfation.

Since there is residual salt from the production process of CNCs and the salt concentrations used in our study are low, we then dialyzed the CNCs for seven days, changing the dialysis water each day. Before pouring the suspension into dialysis tubes, we vacuum-filtered the suspension with a 0.7-micron glass microfiber Whatman filter paper [41]. In all cases, the conductivity of the dialysis water was measured each day and, by the last day, reached that of the deionized water: 0.055 µS/cm (18.2 M$\Omega \cdot$ cm).

Heavy kaolin powder with maximum chloride and sulfate amounts of 250 and 1000 mg/kg, respectively, was purchased from Sigma-Aldrich (Canada, Oakville, ON). 100 mL of the powder dispersion was stirred in a 200 mL beaker at 100 RPM with a 30×6 mm magnetic stirrer for one hour. Then, the dispersion was probe-sonicated for ten minutes with 60% amplitude on a 1/8" microtip in an ice bath (to prevent water evaporation) to form a translucent suspension. Laser diffraction analysis using a SYNC Microtrac (U.S., York, PA) on the suspension reveals that the kaolin particle size is in the range of 1 to 10 µm, with a peak around 3 µm. Measurements show that D50 and D90 for kaolin particles are 3.198 µm and 9.178 µm, respectively.

Spherical silica particles were purchased from U.S. Silica, Inc. (United States, Katy, TX). The procedure for dispersing silica particles in water is similar to that for kaolin particles. We made an initial dispersion by stirring the mixture of the powder at 100 RPM in water for at least one hour using a 30×6 mm magnetic stirrer, followed by probe sonication with the same setting as that used for kaolin. According to laser diffraction, the particle size in the suspension ranges from 1 to 3 µm, with a noticeable peak around 2 µm. Measurements show that D50 and D90 for silica particles are 1.842 µm and 2.883 µm, respectively.

Janus silica particles were prepared at Lehigh University employing the procedure briefly explained here [42]. A silica particle suspension with a surface-area-weighted average diameter, $D_{3,2}$, of 1 µm was deposited as a monolayer roll to roll by Automated Langmuir-Blodget deposition. The first coating of 50 nm Ni is then applied to the top half of the particle monolayer using e-beam

TABLE I. Different surfactant and particle systems with their corresponding droplet and continuous phases.

Surfactantor particle	Droplet phase	Continuous phase
TX-165	Mineral oil	Water
SDS	Mineral oil	Water
Span 80	Water	Mineral oil
Silica	Mineral oil	Water
Janus silica	Mineral oil	Water
Clay	Mineral oil	Water
CNC	Mineral oil	Water
CNC	Mineral oil	1, 10, 100 mM NaCl solution
None added	Diluted bitumen	Water
None added	Diluted bitumen	Simulated process water

evaporation. A 10 nm Au coating is then applied on top of the Ni coating using an e-beam evaporator and the Janus particles are formed [43].

Bitumen used in our study was supplied by Connacher Oil and Gas Inc. (Canada, Calgary, AB). The bitumen is diluted with Naphtha at 4:1 mass ratio to obtain the material commonly referred to as dilbit. At 15 °C, dilbit has a viscosity of 350 cP and density of 0.925 g/cm^3. Dilbit droplet coalescence experiments were done in both deionized water and simulated process water. A solution meant to mimic process water found in one step of the refining of bitumen [24], denoted as simulated process water, is used in this study and is composed of deionized water containing 25 mM NaCl, 15 mM NaHCO$_3$, and 2 mM Na$_2$SO$_4$ with a pH of 8.2.

The concentration of surfactants and particles used in each set of experiments was chosen according to experimental convenience. Specifically, the concentrations were systematically lowered until the coalescence times were on the order of 300 seconds or less. All surfactants and particles with their corresponding droplet and continuous phases are given in Table I.

B. Coalescence experiments

A Cantilevered Capillary Force Apparatus (CCFA) [27,44–50] was used to perform droplet-droplet collision experiments. The instrument contains two capillaries that can be submerged in a liquid, and the flow into and out of the capillary is adjusted by a pressure controller (Elveflow, Paris, France). One of the capillaries is integrated with a piezoelectric stage (Thorlabs, Inc., U.S.), capable of moving with constant velocity and oscillating sinusoidally with a precision of around 5 nm.

Using the CCFA, we were able to hold two droplets of the dispersed phase on the tip of the capillaries and make them interact while submerged in the continuous phase. After positioning the droplets on the capillary tips, a certain amount of time was needed to allow for the migration of surface-active components to the interface to reach equilibrium. The value of the rest time needed was determined from dynamic surface tension data using a Pendant Droplet Tensiometer. For SDS and Triton X-165, a five-minute wait time was used, and for Span 80 and all particles a ten-minute wait time was used. Cameras with orthogonal views of the droplets were used to align the capillaries and record the droplet interaction.

As shown in Fig. 1, two different droplet collision types were used. For both collision types, the droplet diameter, D, was kept constant and equal to 100 ± 2.5 μm and the initial horizontal separation was 100 μm ($L = 200$ μm). Also, for both collision types, the rigid capillary moved toward the cantilevered capillary with a velocity of 10 μm/s until $L = 90$ μm. For what we denote as head-on collisions, there was no axial offset between the droplets ($H = 0$ μm), while for what we denote as shearing collisions, which is a combination of compression and shear, the offset was set to $H = 50$ μm so θ is equal to 30° when the droplets first come into contact. Finally, for shearing collisions, after the initial forward motion, the rigid capillary moved with a sinusoidal profile with an
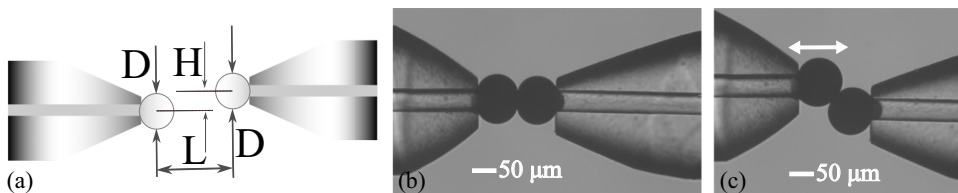
FIG. 1. (a) A schematic showing the geometric parameters used to define the collision of two emulsion droplets. (b) Two dilbit droplets in contact in the head-on configuration ($H = 0$). (c) Two dilbit droplets in contact during an oscillatory shearing collision ($H = 50\,\mu m$). See video in Supplemental Material [51]. Note that the time-averaged droplet contact area in the shear configuration ($1025\,\mu m^2$) is approximately the same as the contact area in the head-on configuration ($1060\,\mu m^2$).

amplitude of 5 μm and frequency of 2 Hz. Note that throughout the shearing collisions, the droplets remain compressed against each other, resulting in a force in the axial direction, as well as a film area between the droplets, that varies periodically with time throughout the contact time.

Depending on the type of emulsion stabilizer, the resulting interfacial tension, and the collision type, the average horizontal force between the droplets ranged from 200–350 nN during a shearing collision and was higher at around 600 nN for head-on collisions. The force was measured by detecting the capillary deflection with a laser; more details on this can be found in Ref. [27]. For both collision types, the coalescence time was measured from the time at which the droplets first come into contact ($L = 100\,\mu m$) to the time that they coalesce. Because of the stochastic nature of the coalescence process when the drainage time is not the dominant timescale [52–54], it is common practice to present the coalescence time data as a cumulative probability distribution. The same approach was adopted here and all distributions are generated from at least 20 repeats for each condition.

C. Droplet generation

To ensure that the droplet diameter was stable over very long periods of time, a unique droplet generation method was developed and validated. The two approaching capillaries were filled with the continuous phase, and small volumes of the dispersed phase were dispensed from an auxiliary capillary filled with the dispersed phase, as shown in Fig. 2. Then, the pressure was controlled to suck the desired volume of the dispersed phase into each of the two capillaries. Afterward, the auxiliary capillary was moved away and the droplets were extruded to the ends of the capillaries
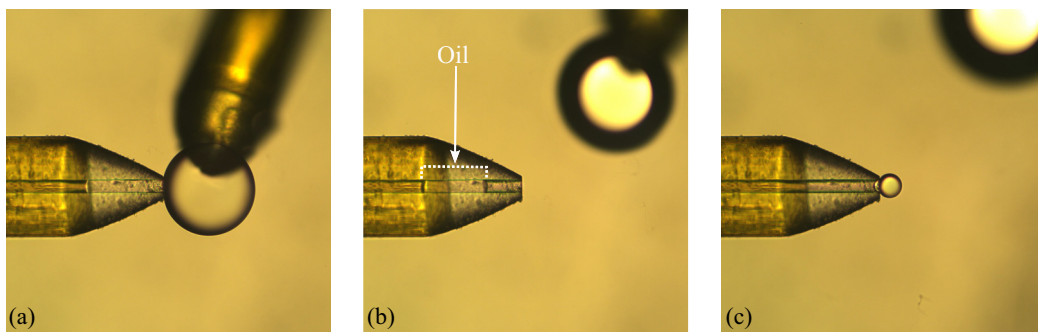

FIG. 2. (a) An oil droplet is formed at the tip of the auxiliary capillary (upper capillary in images) with the chamber and capillaries filled with an aqueous solution. (b) A small amount of oil is sucked into the left capillary. (c) The auxiliary capillary is moved away and an oil droplet is then extruded at the tip of the capillary. The inner diameter of the left capillary is 50 μm.

where they were held in place with a small suction pressure of approximately 10 mbar. Using this method, the droplet diameters were found to vary by less than 0.2% for up to 400 s (we did not measure it longer).

After each coalescence event, one of two protocols was followed. In the case of systems with solid particles, the chamber was completely emptied, rinsed first with isopropyl alcohol and then water, and dried before refilling the chamber and placing the next two droplets on the tips of the capillaries. This protocol ensured that the buildup of particles is not an issue and that the initial conditions are repeatable. In the case of systems with small molecule surfactants, the coalesced droplet was reused by breaking it into two equally sized droplets by applying the same amount of suction in both capillaries, rather than making new droplets via the auxiliary capillary. This protocol was more convenient and yielded reproducible results for the surfactants that we studied.

III. RESULTS AND DISCUSSION

In this section, we first compare the coalescence time for shearing and head-on droplet collisions for surfactant-coated droplets (Sec. III A). As a reminder, our hypothesis is that no difference will be observed and that these results will serve as a control for comparing with more complex compositions. Following surfactant-coated droplets, we present coalescence data for diluted bitumen droplets (dilbit) in either pure water or simulated process water to attempt to reproduce the earlier results of Yeung *et al.* [24] (Sec. III B). Finally, we report coalescence data for droplets coated with four different types of particles to search for other systems where shear-triggered coalescence might be observed (Secs. III C and III D).

To determine the relative importance of hydrodynamic drainage on the timescale for coalescence, we estimated the hydrodynamic drainage time for droplets in our system using the following equation, where it is assumed that the droplet interfaces have a zero-velocity boundary condition [55]:

$$t_d \sim F^{1/4} R^{7/4} \big[\mu \gamma^{-3/4} A_H^{-1/2} \big]. \tag{1}$$

In Eq. (1), F is the force between droplets in contact, R is the droplet radius, μ is the continuous phase viscosity, γ is the interfacial tension, and A_H is the Hamaker constant. Substituting the relevant values, we obtain a drainage time on the order of 0.1 s. However, the range of coalescence times in our study is generally much higher than this. Thus, we conclude that factors related to the size of, and disjoining pressure within the film, rather than hydrodynamic drainage, are dominant in determining the coalescence time [53,54].

A. Surfactant-coated droplets

In this section, we show the coalescence results for droplets stabilized by surfactants. As mentioned before, the main aim of this section is to compare the influence of the collision type on the coalescence time. Here it is worth noting that it is *not* our goal to produce equivalent collisions from the point of view of dimensional analysis. For example, we do not attempt to match the Capillary number (or other dimensionless force parameters) between head-on and shearing collisions. Instead, our goal is to have fixed collision protocols that are both similar to the previous work of Yeung *et al.* and reproducible for making quantitative comparisons between droplets with different compositions. Many other collision protocols could be employed and compared, but that is beyond the scope of the present paper.

The surfactants were selected so they were either ionic (SDS) or nonionic (Triton X-165 and Span 80), and either water soluble (Triton X-165) or oil-soluble (Span 80). Fig. 3 shows the coalescence time as a cumulative distribution for water droplets in oil with 0.05%v/v Span 80, as well as oil droplets in aqueous solutions of either 2 μM Triton X-165 or 1 μM SDS, all much lower than their CMC values. Note that oil droplets in water (with no surfactants added) coalesce immediately after contact, and this is one way that we verified that the chamber is clean between experiments.
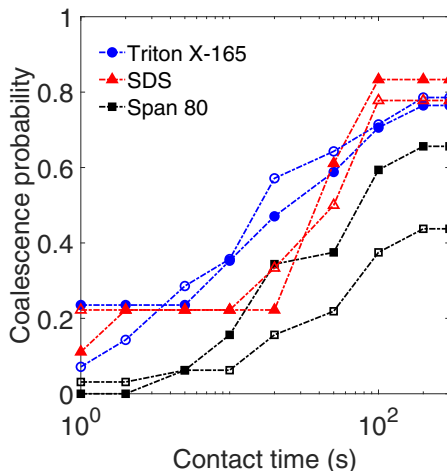
FIG. 3. Cumulative distribution for the probability of coalescence for water droplets in light mineral oil containing 0.05 %v/v Span 80, light mineral oil droplets in 0.002 mM aqueous Triton X-165 solution, and light mineral oil droplets in 0.001 mM aqueous SDS solution. Filled and unfilled symbols denote head-on and shearing collisions, respectively.

From these data, we conclude that there is either only a very minor difference between head-on and shearing collisions or that the coalescence is actually faster for head-on collisions than for shearing collisions (opposite to shear-triggered coalescence) regardless of the surfactant type or droplet type. In the latter case, which is observed distinctly for the water droplets in oil with Span 80, the faster coalescence in the head-on collision might be related to the differences in the magnitude of the collision force (i.e., it is lower for a shearing collision), but more work is needed to explain the effect. Otherwise, this confirms our hypothesis that surfactant systems do not exhibit shear-triggered coalescence and can serve as a good control for showing evidence of shear-triggered coalescence.

B. Diluted bitumen (dilbit) coalescence results

After confirming the validity of our method for varying the collision type, we attempted to employ it to observe shear-triggered coalescence with bitumen droplets (as in the original study by Yeung *et al.* [24]). Unfortunately, flowing bitumen through our capillaries at ambient conditions was almost impossible due to its very high viscosity, so instead we used bitumen diluted with Naphtha for our experiments (commonly referred to as dilbit). The dilbit droplets collided in either water or in simulated process water with the same composition used in Ref. [24]. Thus, both conditions represent an O/W emulsion. Note that the simulated process water is intended to simulate the water found during processing of bitumen.

Interestingly, we found that the dilbit droplets in simulated process water do not coalesce even after being in contact for up to six hours. On the other hand, in water, the majority of dilbit droplets coalesced between 0 to 300 seconds. While we do observe coalescence without salt, Fig. 4 shows that there is no evidence of shear-triggered coalescence in either case. Instead there is a slightly lower probability of coalescence for the sheared case in water, possibly due to the lower interaction force caused by the offset of the capillaries, as discussed previously. The lack of coalescence in the simulated process water might be related to the higher pH influencing the interfacial properties, but more work is needed to explain this result.

There are a couple of factors worth mentioning that might be responsible for the lack of shear-triggered coalescence with dilbit droplets. First, it is well-known that the composition of bitumen is highly variable, so there is little chance that the materials used here are identical to those
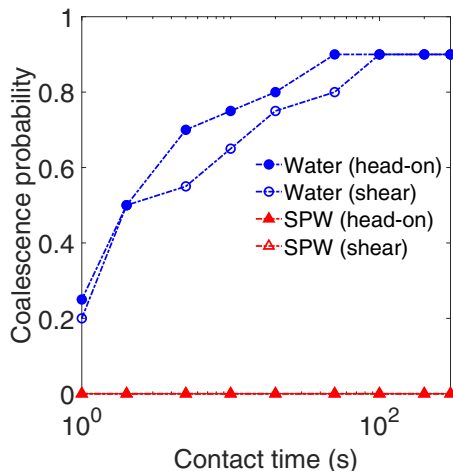
FIG. 4. Cumulative distribution for the probability of coalescence of dilbit droplets in deionized water or simulated process water (SPW). Filled and unfilled symbols denote head-on and shearing collisions, respectively.

used in prior work. Second, diluting bitumen with naphtha will certainly alter the physicochemical properties such as viscosity (which drops by several orders of magnitude), interfacial tension, arrangement of charges, and fluidity of molecules and aggregates at the interface. Both of these issues were known in advance of our work, but we had hoped that shear-triggered coalescence would still be observed. Nevertheless, we maintain our hypothesis that shear-triggered coalescence can be observed in a simple system.

C. Particle-stabilized droplets: Rotating particle mechanism

Similar to surfactant molecules, micro- or nanoscale particles can sit at fluid-fluid interfaces, preventing coalescence by forming either a steric or repulsive barrier. Unlike surfactants, the particle desorption energy is so high that they are considered irreversibly adsorbed components. If the particles are spherical, they can rotate due to shear flow in the film or hard contact with another particle as the droplets slide past each other [56].

If the contact line from the interface happens to be pinned on the particle, we hypothesize that this could distort the interfaces and bring the interfaces close enough together to trigger coalescence as in the cartoon depiction in Fig. 5(a). However, we expect that the shape of the particle and the value of the contact angle will influence the possibility of this event. Therefore, we also test platelike clay particles that will not rotate, as well as bare silica particles that have a lower contact angle.

To check if this particle rotation mechanism is in the realm of physical possibility, we performed a scaling analysis to compare the two major torques involved in a particle under shear. The torque causing particle rotation can originate from the shear stress in the bulk fluid [57], while the torque opposing the droplet rotation is caused by surface tension [58,59]. Writing these two torques as a dimensionless ratio, we have

$$\frac{T_{\text{shear}}}{T_{\text{tension}}} = \frac{\mu \dot{\gamma} a^3}{\sigma a^2}. \tag{2}$$

Here, μ is the bulk phase viscosity, $\dot{\gamma}$ is the shear rate, a is the particle radius, and σ is the interfacial tension between mineral oil and water.

With Eq. (2), we can use order-of-magnitude estimates of each quantity to determine if the particle rotation mechanism is feasible. The maximum possible shear rate caused by the flow can be
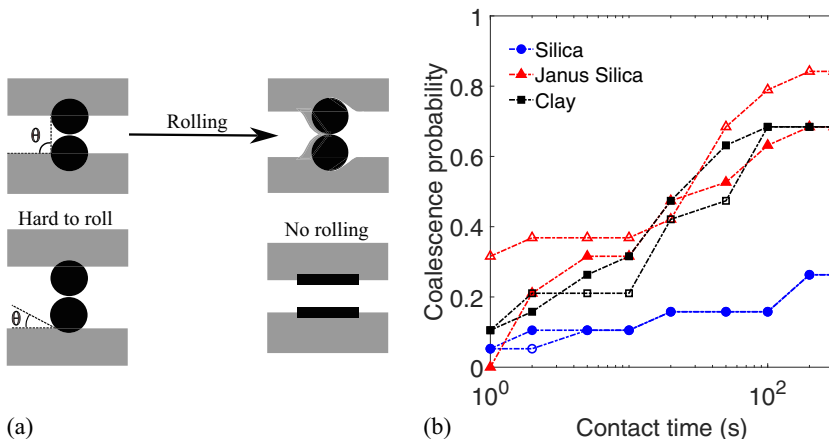
FIG. 5. (a) Upper: A schematic showing how spherical particles with a contact line pinned at 90º (e.g., the spherical Janus microparticles used in this study) might roll during a shearing collision to drag a thin layer of oil and facilitate bridging between the two droplets. (a) Lower: A schematic showing the two other particles used in this study that do not roll (disklike clay microparticles) or might roll without sufficient distortion of the interface to trigger coalescence (spherical silica microparticles). (b) Cumulative distribution for the probability of coalescence of mineral oil droplets in 0.001 wt% silica suspension, 0.0001 wt % Janus silica suspension, and 0.0007 wt % clay suspension. Filled and unfilled symbols denote head-on and shearing collisions, respectively.

estimated by the relative droplet velocity divided by the minimum gap width: $10^{-5}/10^{-8} = 10^3 \, 1/s$. The surface tension is $O(10^{-2})$ and the particle size is $O(10^{-6})$. With these estimates, we see that the torque from the shear flow is three to four orders of magnitude smaller than the torque required to rotate the particle.

Thus, we see that a shear flow field due to the particles sliding past each other is highly unlikely to produce the particle rotation mechanism. However, as mentioned above, it is also possible that particles on opposing droplets can come into solid-body contact. In that case, we hypothesize that there still exists the possibility of particle rotation during a shearing collision.

To test our hypothesis, we produced head-on and shearing collisions of oil droplets in aqueous suspensions of three types of particles. Two of the particles were spherical with differing wettability (and therefore contact angle) and size and the other was platelike. The platelike particles are included as a control that is not expected to rotate significantly.

Knowing that the optimal contact angle for a particle to stabilize an emulsion droplet is $90°$, and also noting that this condition is ideal for particle rotation to bridge the gap between particles, we employed Janus particles that are half hydrophilic and half hydrophobic. As shown in Fig. 5(b), we see an apparent difference in head-on vs shearing collisions, with faster coalescence times for shearing. However, the observed difference is not quite statistically significant for this number of measurements (see Table II), and it is certainly not as dramatic a difference as observed in the prior work.

Additionally, we see the interesting result that the probability distribution appears to be bimodal for the shearing collisions and more monomodal for the head-on collisions. Conducting Hartigan's dip test on each of these distributions resulted in a p value of 0.08 and 0.15 for shear and head-on distributions, respectively, indicating bimodality with marginal significance for the shearing collision and monomodality for the head-on collision. At present, we are not able to offer an explanation for the bimodal nature of the coalescence times, though it definitely points to a difference in the nature of the mechanism causing coalescence in the two cases. To conclude that this is proof of our hypothesized mechanism would be inappropriate, but at least we can say that the evidence does not

TABLE II. Statistical significance of the difference between the coalescence probability distributions for head-on and shearing collisions for selected systems from those investigated. The *p* values obtained from three different statistical tests are presented below, and in each case a *p* value of less than 0.05 indicates a statistically significant difference. A * indicates that a significant difference was observed for that system.

Test name	p-value							CNC*
	TX-165	SDS	Span 80*	Diluted bitumen in water	Clay	Silica	Janus silica	CNC*
Kolmogorov-Smirnov	0.75	0.78	0.27	0.83	0.81	0.99	0.15	4.2×10^{-6}
Mann-Whitney U test	0.3	0.4	0.02	0.25	0.2	0.48	0.09	1.2×10^{-5}
Z test	0.9	0.72	0.05	0.69	0.49	0.96	0.3	2.6×10^{-11}

contradict it. We also note that Janus microparticles have been hypothesized to behave differently from isotropic particles in other ways as well [60].

As another test of the mechanism, we used bare, spherical silica particles and found that they are more effective at stabilizing oil droplets than the Janus particles (see Fig. 5). Comparing the head-on and shear coalescence probability, we see a minimal difference between the two collision types and therefore no shear-triggered coalescence. To explain this result, we note that, unlike the Janus particles, the entire particle surface is hydrophilic and the three-phase contact angle for particles at the oil-water interface will be significantly lower than $90°$. Because of that, the aqueous phase wets a greater portion of the particle, requiring the particle to rotate to a much larger degree to bring the interfaces into contact. As a result, the applied shear appears not to be sufficient to trigger coalescence and we suspect that the larger particle size may result in the more effective stabilization due to an increased steric barrier.

With the platelike clay particles, we expect that neither shear forces nor hard contact will be sufficient to cause any rotation of the particle [as shown in Fig. 5(a)] and so shear-triggered coalescence should not be observed. Indeed, as shown in Fig. 5(b), the clay particles also do not show evidence of shear-triggered coalescence. Again, while these data are not conclusive in establishing the rotation mechanism, they do not contradict that mechanism and do suggest that particle morphology can be tuned to produce shear-triggered coalescence.

D. Particle-stabilized droplets: Particle orientation mechanism

In addition to the potential for spherical particles to rotate, we hypothesize that rod-shaped particles can be oriented on the interface by the flow. If the surface coverage of the droplet is not too high, the reorientation could lead to more efficient packing on the interface and leave some uncovered interface where coalescence can be triggered. To test this hypothesis, we study rod-shaped CNCs, which have recently been used as promising emulsion stabilizers [61–65].

We first employed a 0.04 wt % CNC suspension in deionized water to stabilize mineral oil droplets. The concentration is high enough to fully cover the droplets [62]. Even though we performed 20 trials for each of the head-on and shearing scenarios, no droplet coalescence was observed for five minutes of contact.

Previous CNC characterization shows that CNCs suspended in water are negatively charged, so there is a strong electrostatic repulsive force between CNC particles. When many CNCs are adsorbed at the interface, the net charge on the droplets can be sufficient to act as an electrostatic barrier against coalescence [66]. Therefore, in the next step, we added NaCl to the CNC solution to screen charges and reduce the electrostatic force.

We chose three different salt concentrations while keeping the CNC concentration constant. As shown in Fig. 6(a), similar to the case without salt, low salt (1 mN NaCl) and high salt (100 mM NaCl) concentrations did not allow any coalescence in either of the two different collision scenarios.
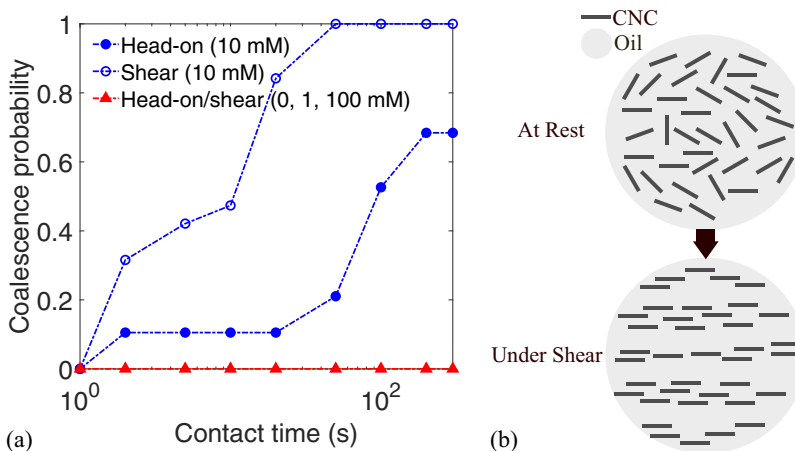
FIG. 6. (a) Cumulative distribution for the probability of coalescence for mineral oil droplets in 0.04 wt % cellulose nanocrystals in 0, 10, and 100 mM NaCl solution. Filled and unfilled symbols denote head-on and shearing collisions, respectively. (b) A schematic showing how cellulose nanocrystals might reorient and align during a shearing interaction in the presence of 10 mM NaCl.

However, when we added 10 mM NaCl to the CNC suspension, as shown in Fig. 6(a), not only did we observe more than two times higher coalescence probabilities for the shearing case (compared with head-on collisions), but also all the droplet pairs under shear coalesced in under 50 seconds.

Thus, there is obviously a nonmonotonic trend in the coalescence probability as a function of the salt concentration. We suggest the following explanation for this effect. At very low salt concentrations, the CNCs are spaced relatively far apart on the interface, but still prevent coalescence by electrostatic repulsion between the droplets due to a large Debye length. On the other hand, high salt concentrations screen the charges between CNCs to such an extent that CNCs can fully coat the interface and act as a strong steric barrier, preventing coalescence.

However, we suggest that there is a sweet spot at intermediate salt concentration where the electrostatic force is not high enough to prevent coalescence (decreased Debye length) but there remains enough electrostatic repulsion to maintain some space between particles on the interface. This picture is consistent with calculations of the Debye length (not presented) as well as rheological measurements on CNC dispersions in this range of salt concentrations [67]. In this configuration, the interfacial coverage would be enough to provide a barrier against coalescence, yet the extra space between randomly oriented particles can be consolidated through ordering by a shear flow as shown in Fig. 6(b). This reorientation and consolidation could then leave some fresh interface on oil droplets where there is no barrier to coalescence.

Thus, in effect, surface heterogeneity may be responsible for lowering the barrier for coalescence, and shearing may enhance the heterogeneity enough to trigger coalescence. As with the previous mechanism, our data suggest that this mechanism is correct, but are insufficient to prove it. Still, alternate explanations are possible, and it is worth noting that interfacial rheology may play an important role by, for example, presenting a critical interfacial strain above which interfacial layers can rupture leading to coalescence [68]. Nevertheless, we have clearly made a dramatic demonstration of the existence of shear-triggered coalescence, showing at least an order of magnitude increase in the rate of coalescence.

To further quantify the difference between coalescence probability for head-on and shearing collisions, we performed three statistical tests as shown in Table II. The null hypothesis for all tests is that both distributions are the same and there is no significant difference between them. With that, we calculated p values for different systems in our study, where if the p value is greater than 0.05, there is not enough evidence to reject the null hypothesis. Notably, the results of these tests confirm

that for water droplets in mineral oil with Span 80, coalescence is significantly faster in the head-on configuration, and for mineral oil droplets stabilized by CNC particles in 10 mM NaCl solution, coalescence is significantly faster for shearing collisions.

IV. CONCLUSION

In an attempt to better understand the shear-triggered coalescence observed in a previous study [24], we developed a method to systematically compare head-on vs shearing collisions between two isolated emulsion droplets. Consistent with one of our hypotheses, we conclude that three different small-molecule surfactants show no difference in the coalescence probability when comparing the two collision types. Further, droplets of bitumen diluted with solvent did not exhibit shear-triggered coalescence in deionized water or in simulated process water. However, we did observe shear-triggered coalescence for oil droplets coated with two different types of particles: spherical, Janus microparticles, and rod-shaped nanoparticles. From this, we conclude that two different mechanisms (particle rotation and particle reorientation) may be capable of resulting in shear-triggered coalescence. These results show that solid particles can be selected and/or designed to achieve both quantitative and qualitative differences in the coalescence probability for droplets colliding head-on vs under shear.

[1] D. J. Mcclements, Critical review of techniques and methodologies for characterization of emulsion stability, Crit. Rev. Food Sci. Nutr. **47**, 611 (2007).

[2] T. M. Ho, A. Razzaghi, A. Ramachandran, and K. S. Mikkonen, Emulsion characterization via microfluidic devices: A review on interfacial tension and stability to coalescence, Adv. Colloid Interface Sci. **299**, 102541 (2022).

[3] D. Langevin, Coalescence in foams and emulsions: Similarities and differences, Curr. Opin. Colloid Interface Sci. **44**, 23 (2019).

[4] A. Håkansson, Experimental methods for measuring coalescence during emulsification—A critical review, J. Food Eng. **178**, 47 (2016).

[5] F. Ravera, K. Dziza, E. Santini, L. Cristofolini, and L. Liggieri, Emulsification and emulsion stability: The role of the interfacial properties, Adv. Colloid Interface Sci. **288**, 102344 (2021).

[6] J. S. Eow, M. Ghadiri, A. O. Sharif, and T. J. Williams, Electrostatic enhancement of coalescence of water droplets in oil: A review of the current understanding, Chem. Eng. J. **84**, 173 (2001).

[7] L. E. Low, S. P. Siva, Y. K. Ho, E. S. Chan, and B. T. Tey, Recent advances of characterization techniques for the formation, physical properties and stability of Pickering emulsion, Adv. Colloid Interface Sci. **277**, 102117 (2020).

[8] Z. Liu, S. T. Chan, H. A. Faizi, R. C. Roberts, and H. C. Shum, Droplet-based electro-coalescence for probing threshold disjoining pressure, Lab Chip **15**, 2018 (2015).

[9] S. Goel and A. Ramachandran, The suppression of droplet-droplet coalescence in a sheared yield stress fluid, J. Colloid Interface Sci. **492**, 199 (2017).

[10] D. Georgieva, V. Schmitt, F. Leal-Calderon, and D. Langevin, On the possible role of surface elasticity in emulsion Sstability, Langmuir **25**, 5565 (2009).

[11] M. M. Abdulredha, S. A. Hussain, L. C. Abdullah, and T. L. Hong, Water-in-oil emulsion stability and demulsification via surface-active compounds: A review, J. Pet. Sci. Eng. **209**, 109848 (2022).

[12] A. P. Udepurkar, C. Clasen, and S. Kuhn, Emulsification mechanism in an ultrasonic microreactor: Influence of surface roughness and ultrasound frequency, Ultrason. Sonochem. **94**, 106323 (2023).

[13] V. Konovalova, I. Kolesnyk, M. Savchenko, A. Marynin, H. Bubela, J. Kujawa, K. Knozowska, and W. Kujawski, Preparation of chitosan water-in-oil emulsions by stirred cell membrane emulsification, Colloids Surf., A **661**, 130929 (2023).

[14] G. Øye, S. Simon, T. Rustad, and K. Paso, Trends in food emulsion technology: Pickering, nano-, and double emulsions, Curr. Opin. Food Sci. **50**, 101003 (2023).

[15] J. D. dos Santos Carvalho, R. S. Rabelo, K. F. Cerqueira e Silva, and M. D. Hubinger, Oil-in-water emulsion gels stabilized with cellulosic polymers and chitosan: Themorheological and physical-chemical evaluation, Int. J. Biol. Macromol. **236**, 123828 (2023).

[16] X. Yao, R. Lin, Y. Liang, S. Jiao, and L. Zhong, Characterization of acetylated starch nanoparticles for potential use as an emulsion stabilizer, Food Chem. **400**, 133873 (2023).

[17] S. Narayan, A. E. Metaxas, R. Bachnak, T. Neumiller, and C. S. Dutcher, Zooming in on the role of surfactants in droplet coalescence at the macroscale and microscale, Curr. Opin. Colloid Interface Sci. **50**, 101385 (2020).

[18] N. Bremond, A. R. Thiam, and J. Bibette, Decompressing emulsion droplets favors coalescence, Phys. Rev. Lett. **100**, 024501 (2008).

[19] M. Dudek, J. Chicault, and G. Øye, Microfluidic investigation of crude oil droplet coalescence: Effect of oil/water composition and droplet aging, Energy Fuels **34**, 5110 (2020).

[20] Q. Zhou, Y. Sun, S. Yi, K. Wang, and G. Luo, Investigation of droplet coalescence in nanoparticle suspensions by a microfluidic collision experiment, Soft Matter **12**, 1674 (2016).

[21] A. Razzaghi and A. Ramachandran, Controlled collision of Hele-Shaw drops in extensional flow using a six-port microfluidic device, Phys. Rev. Fluids **8**, 084201 (2023).

[22] E. Chatzigiannakis, P. Veenstra, D. ten Bosch, and J. Vermant, Mimicking coalescence using a pressure-controlled dynamic thin film balance, Soft Matter **16**, 9410 (2020).

[23] M. Tanyeri, M. Ranka, N. Sittipolkul, and C. M. Schroeder, A microfluidic-based hydrodynamic trap: Design and implementation, Lab Chip **11**, 1786 (2011).

[24] A. Yeung, K. Moran, J. Masliyah, and J. Czarnecki, Shear-induced coalescence of emulsified oil drops, J. Colloid Interface Sci. **265**, 439 (2003).

[25] L. Zhang, C. Shi, Q. Lu, Q. Liu, and H. Zeng, Probing molecular interactions of asphaltenes in heptol using a surface forces apparatus: Implications on stability of water-in-oil emulsions, Langmuir **32**, 4886 (2016).

[26] O. Aarøen, E. Riccardi, and M. Sletmoen, Exploring the effects of approach velocity on depletion force and coalescence in oil-in-water emulsions, RSC Adv. **11**, 8730 (2021).

[27] J. M. Frostad, M. C. Collins, and L. G. Leal, Cantilevered-capillary force apparatus for measuring multiphase fluid interactions, Langmuir **29**, 4715 (2013).

[28] J. M. Frostad, D. Tammaro, L. Santollani, S. Bochner De Araujo, and G. G. Fuller, Dynamic fluid-film interferometry as a predictor of bulk foam properties, Soft Matter **12**, 9266 (2016).

[29] H.-H.-Q. Dinh, E. Santanach-Carreras, M. Lalanne-Aulet, V. Schmitt, P. Panizza, and F. Lequeux, Effect of a surfactant mixture on coalescence occurring in concentrated emulsions: The hole nucleation theory revisited, Langmuir **37**, 8726 (2021).

[30] P. Esmaeili, F. Lin, and A. Yeung, Stability of emulsified heavy oil: The combined effects of deterministic DLVO forces and random surface charges, Langmuir **28**, 4948 (2012).

[31] J. Drelich and X. Yin, Mapping charge-mosaic surfaces in electrolyte solutions using surface charge microscopy, Appl. Surf. Sci. **256**, 5381 (2010).

[32] C. P. Whitby, F. E. Fischer, D. Fornasiero, and J. Ralston, Shear-induced coalescence of oil-in-water Pickering emulsions, J. Colloid Interface Sci. **361**, 170 (2011).

[33] J. Legrand, M. Chamerois, F. Placin, J. E. Poirier, J. Bibette, and F. Leal-Calderon, Solid colloidal particles inducing coalescence in bitumen-in-water emulsions, Langmuir **21**, 64 (2005).

[34] G. A. Van Aken and T. Van Vliet, Flow-induced coalescence in protein-stabilized highly concentrated emulsions: Role of shear-resisting connections between the droplets, Langmuir **18**, 7364 (2002).

[35] E. Davies, E. Dickinson, and R. Bee, Shear stability of sodium caseinate emulsions containing monoglyceride and triglyceride crystals, Food Hydrocoll. **14**, 145 (2000).

[36] S. Zhang, L. Zhang, X. Lu, C. Shi, T. Tang, X. Wang, Q. Huang, and H. Zeng, Adsorption kinetics of asphaltenes at oil/water interface: Effects of concentration and temperature, Fuel **212**, 387 (2018).

[37] J. You, C. Li, D. Liu, F. Yang, and G. Sun, Influence of the aggregation state of asphaltenes on structural properties of the model oil/brine interface, Energy Fuels **33**, 2994 (2019).

[38] M. R. Gray, H. W. Yarranton, M. L. Chacón-Patiño, R. P. Rodgers, B. Bouyssiere, and P. Giusti, Distributed properties of asphaltene nanoaggregates in crude oils: A review, Energy Fuels **35**, 18078 (2021).

[39] J. G. Alvarado, J. G. Delgado-Linares, A. M. Forgiarini, and J.-L. Salager, Breaking of water-in-crude oil emulsions. 8. Demulsifier performance at optimum formulation is significantly improved by a small aromatic content of the oil, Energy Fuels **33**, 1928 (2019).

[40] C. Shi, L. Zhang, L. Xie, X. Lu, Q. Liu, J. He, C. A. Mantilla, F. G. A. Van den berg, and H. Zeng, Surface interaction of water-in-oil emulsion droplets with interfacially active asphaltenes, Langmuir **33**, 1265 (2017).

[41] A. S. Pakdel, V. Gabriel, R. M. Berry, C. Fraschini, E. D. Cranston, and M. A. Dubé, A sequential design approach for in situ incorporation of cellulose nanocrystals in emulsion-based pressure sensitive adhesives, Cellulose **27**, 10837 (2020).

[42] T. Muangnapoh, A. L. Weldon, and J. F. Gilchrist, Enhanced colloidal monolayer assembly via vibration-assisted convective deposition, Appl. Phys. Lett. **103**, 181603 (2013).

[43] C. Shen, Z. Jiang, L. Li, J. F. Gilchrist, and H. D. Ou-Yang, Frequency response of induced-charge electrophoretic metallic janus particles, Micromachines **11**, 334 (2020).

[44] J. M. Frostad, M. Seth, S. M. Bernasek, and L. G. Leal, Direct measurement of interaction forces between charged multilamellar vesicles, Soft Matter **10**, 7769 (2014).

[45] J. M. Frostad, M. C. Collins, and L. G. Leal, Direct measurement of the interaction of model food emulsion droplets adhering by arrested coalescence, Colloids Surf., A **441**, 459 (2014).

[46] P. Safieh, D. J. Walls, J. M. Frostad, A. G. Marangoni, S. Mirzaee Ghazani, and E. Pensini, Effect of toluene and hexane sorption on the rheology and interfacial properties of lecithin-based emulsion gels, Langmuir **36**, 1484 (2020).

[47] J. M. Frostad, A. Paul, and L. G. Leal, Coalescence of droplets due to a constant force interaction in a quiescent viscous fluid, Phys. Rev. Fluids **1**, 033904 (2016).

[48] Y.-H. Huang, X. Li, M. Michelon, B. C. Leopercio, M. S. Carvalho, and J. M. Frostad, Effects of aging on the shelf life and viscoelasticity of gellan gum microcapsules, Food Hydrocoll. **121**, 106982 (2021).

[49] Y.-H. Huang, F. Salmon, A. Kamble, A. X. Xu, M. Michelon, B. C. Leopercio, M. S. Carvalho, and J. M. Frostad, Models for the mechanical characterization of core-shell microcapsules under uniaxial deformation, Food Hydrocoll. **119**, 106762 (2021).

[50] C. K. Okwara, R. Vaez Ghaemi, C. Yu, M. Le, V. G. Yadav, and J. M. Frostad, The mechanical properties of neurospheres, Adv. Eng. Mater. **23**, 2100172 (2021).

[51] See Supplemental Material at http://link.aps.org/supplemental/10.1103/PhysRevFluids.9.023602 for representative videos showing a head-on collision and a shearing collision.

[52] P. Ghosh, Coalescence of air bubbles at air-water interface, Chem. Eng. Res. Des. **82**, 849 (2004).

[53] E. Chatzigiannakis, Y. Chen, R. Bachnak, C. S. Dutcher, and J. Vermant, Studying coalescence at different lengthscales: From films to droplets, Rheol. Acta **61**, 745 (2022).

[54] E. Forel, B. Dollet, D. Langevin, and E. Rio, Coalescence in two-dimensional foams: A purely statistical process dependent on film area, Phys. Rev. Lett. **122**, 088002 (2019).

[55] J. M. Frostad, J. Walter, and L. G. Leal, A scaling relation for the capillary-pressure driven drainage of thin films, Phys. Fluids **25**, 052108 (2013).

[56] C. Pozrikidis, Particle motion near and inside an interface, J. Fluid Mech. **575**, 333 (2007).

[57] P. Bagchi and S. Balachandar, Effect of free rotation on the motion of a solid sphere in linear shear flow at moderate Re, Phys. Fluids **14**, 2719 (2002).

[58] A. Naga, D. Vollmer, and H.-J. Butt, Capillary torque on a particle rotating at an interface, Langmuir **37**, 7457 (2021).

[59] A. Naga, H.-J. Butt, and D. Vollmer, The force required to detach a rotating particle from a liquid-fluid interface, Langmuir **37**, 13012 (2021).

[60] J. Lenis, S. Razavi, K. D. Cao, B. Lin, K. Y. C. Lee, R. S. Tu, and I. Kretzschmar, Mechanical stability of polystyrene and janus particle monolayers at the air/water interface, J. Am. Chem. Soc. **137**, 15370 (2015).

[61] M. Massicotte and E. D. Cranston, Comparison of techniques for drying cellulose nanocrystal pickering emulsions into oil powders, ACS Sustainable Chem. Eng. **10**, 14914 (2022).

[62] Z. Hu, S. Ballinger, R. Pelton, and E. D. Cranston, Surfactant-enhanced cellulose nanocrystal Pickering emulsions, J. Colloid Interface Sci. **439**, 139 (2015).

[63] L. Liu, Z. Hu, X. Sui, J. Guo, E. D. Cranston, and Z. Mao, Effect of counterion choice on the stability of cellulose nanocrystal pickering emulsions, Ind. Eng. Chem. Res. **57**, 7169 (2018).

[64] L. Bai, S. Lv, W. Xiang, S. Huan, D. J. McClements, and O. J. Rojas, Oil-in-water Pickering emulsions via microfluidization with cellulose nanocrystals: 1. Formation and stability, Food Hydrocoll. **96**, 699 (2019).

[65] P. Ataeian, Q. Shi, M. Ioannidis, and K. C. Tam, Effect of hydrophobic modification of cellulose nanocrystal (CNC) and salt addition on Pickering emulsions undergoing phase-transition, Carbohydrate Polym. Technol. Appl. **3**, 100201 (2022).

[66] Y. Lu, J. Li, L. Ge, W. Xie, and D. Wu, Pickering emulsion stabilized with fibrous nanocelluloses: Insight into fiber flexibility-emulsifying capacity relations, Carbohydrate Polym. **255**, 117483 (2021).

[67] R. Fournier, M. Caye Díaz, E. D. Cranston, and J. M. Frostad, Apparent failures in interpretation of interfacial characterization when formulating emulsions stabilized by cellulose nanocrystals, Langmuir **39**, 13921 (2023).

[68] P. Bertsch and P. Fischer, Interfacial rheology of charged anisotropic cellulose nanocrystals at the air-water interface, Langmuir **35**, 7937 (2019).